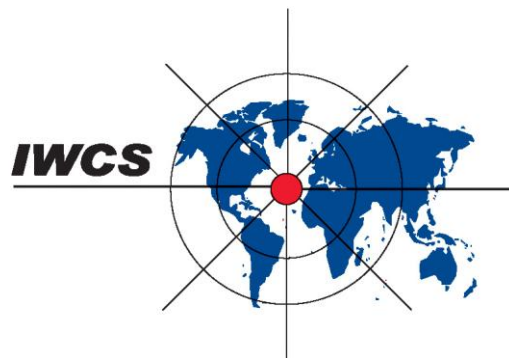


# Transactions of the International Wire & Cable Symposium

**Analytical Mathematical Model for the Calculation of Current Density Distribution Over the Cross-Section of a Multi-conductor Cable**

*K.Q. da Costa, V.Dmitriev, J.T. Pinho, S. Colle, L. Gonzalez, M.A. Andrade, J.C.V. da Silva  
and M.Bedia*

DOI:10.3841/TIWCS.2008.10



2008



# Analytical Model for the Calculation of Current Density Distributions over the Cross-Section of a Multi-Conductor Cable

Karlo Q. da Costa<sup>1</sup>, Victor Dmitriev<sup>1</sup>, João T. Pinho<sup>1</sup>, Sérgio Colle<sup>2</sup>, Luciana Gonzalez<sup>1</sup>, Marcelo A. Andrade<sup>3</sup>, João C. V. da Silva<sup>3</sup>, Mauro Bedia<sup>3</sup>

<sup>1</sup>Department of Electric Engineering / Federal University of Pará  
Belém – Pará – Brazil  
+55-91-32111299 · [karlo@ufpa.br](mailto:karlo@ufpa.br)

<sup>2</sup>Department of Mechanical Engineering / Federal University of Santa Catarina  
Florianópolis – Santa Catarina – Brazil  
+55-48-32342161 · [colle@emc.ufsc.br](mailto:colle@emc.ufsc.br)

<sup>3</sup>Prysmian Telecomunicações Cabos e Sistemas do Brasil S.A.  
Sorocaba – São Paulo – Brazil  
+55-15-32359209 · [marcelo.andrade@prysmian.com](mailto:marcelo.andrade@prysmian.com)

## Abstract

This work presents an analytical model based on Maxwell's equations for current density and electromagnetic field structure calculations in multi-conductor cables. One example of such cables is a composite fiber-optic overhead ground wire (OPGW). A circular multilayer waveguide model is used to represent approximately this cable. The waveguide consists of four layers: dielectric (silica) in the core, aluminum in the intermediate layer, steel in the outer layer and air. The  $TM_{0n}^z$  modes of the waveguide, which have axial symmetry, are analytically analyzed. The numerical results presented here are the dispersion characteristics, the distribution of the electromagnetic fields and the variation of the current density in the cross-section of the waveguide as a function of frequency. This model allows one in particular to investigate the skin effect and the electromagnetic fields inside and outside of the cable.

**Keywords:** OPGW, waveguide model, current density, dispersion characteristics, electromagnetic fields, skin effect.

## 1. Introduction

The multi-conductor cable OPGW is used with a double function of lightning protection for high voltage transmission lines, and as a communications channel through the optical fibers embedded in the cable structure. The optical fiber package is protected by an aluminum tube, which is covered by wires made of steel or steel-aluminum weld. When submitted to short-circuit or lightning conditions, several factors, such as caging, plastic deformations in the tube, disruption and/or destruction of the armored steel wires, can occur in such cables. The calculation of heat distribution in the cross-section of a cable [1] is based on the distribution of current density, which in turn depends on the skin effect. Knowing the current pulse in the cable, one can calculate the spectrum of the pulse, and consequently, the range of frequencies where the most part of the electric power is concentrated. The following analysis of the current density distribution therefore can be fulfilled in the frequency domain. We present in this paper an electrodynamic model of a multiconductor OPGW cable. This model is used for analysis of current density and electromagnetic field distribution in the cable. In our model, the real cable is substituted by a multilayer structure consisting of a dielectric rod, an intermediate aluminum layer and an outer layer of steel. In contrast to earlier publications [2,3], in our analysis we do not introduce the approximation: "in metals, conduction current is much more greater than the displacement current", and this allows one to solve the problems more exactly.

## 2. Mathematical Model

The cross section geometry of the OPGW cable and the corresponding waveguide model are shown in Fig. 1a and Fig. 1b, respectively. The model of Fig. 1b consists of four homogeneous layers: dielectric ( $\rho < a$ ), aluminum ( $a < \rho < b$ ), steel ( $b < \rho < c$ ), and air ( $\rho > c$ ). The metal layers have finite conductivities. The analysis of the waveguide is based on Maxwell's equations in the frequency domain. As a first step, we consider the eigenvalue problem. We shall look for the electromagnetic fields  $TM_{0n}^z$  and the currents which do not have variations with respect to the azimuthal coordinate  $\phi$ , i.e.  $\partial/\partial\phi = 0$ . In the above notation  $TM_{0n}^z$  the member  $n$  is a nonnegative integer.

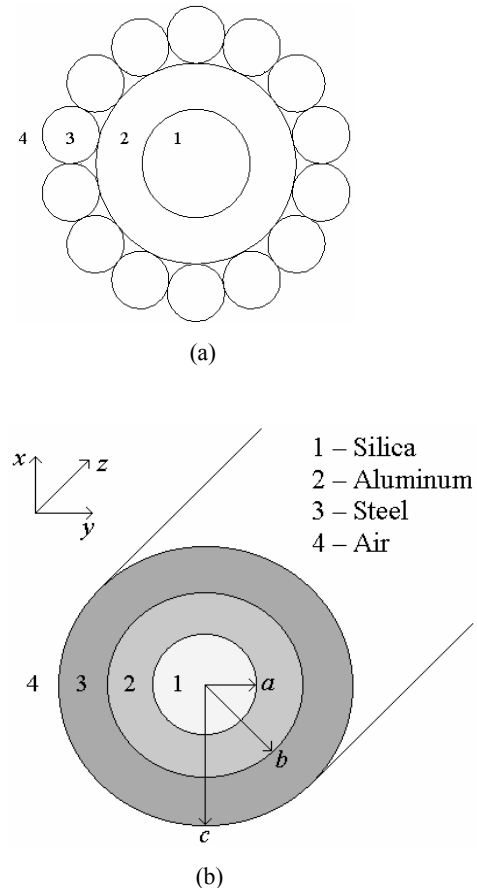


Figure 1. Cross section geometry of the OPGW cable. (a) real geometry. (b) geometry of the analytical model.

## 2.1 General electromagnetic fields solutions

From the Maxwell equations in cylindrical coordinate system in the frequency domain, the set of equations for TM<sup>z</sup> modes for the layers 1-4 shown in Fig. 1 is given by

$$\frac{\partial E_\rho}{\partial z} - \frac{\partial E_z}{\partial \rho} = -j\omega\mu H_\phi \quad (1)$$

$$\frac{\partial H_\phi}{\partial z} = -j\omega\epsilon E_\rho \quad (2)$$

$$\frac{1}{\rho} \frac{\partial(\rho H_\phi)}{\partial \rho} = j\omega\epsilon E_z \quad (3)$$

where  $\omega = 2\pi f$  is the angular frequency,  $f$  is the frequency in Hz,  $\mu$  and  $\epsilon$  are, respectively, the magnetic permeability and the electric permittivity of the layers under consideration (Fig. 1b). Using  $\exp(-jk_z z)$  dependence of the electromagnetic fields, one has:

$$E_\rho(\rho, z) = E_\rho(\rho)e^{-jk_z z} \quad (4)$$

$$E_z(\rho, z) = E_z(\rho)e^{-jk_z z} \quad (5)$$

$$H_\phi(\rho, z) = H_\phi(\rho)e^{-jk_z z} \quad (6)$$

Using the fields in (1)-(3), the following equations are obtained

$$-jk_z E_\rho - \frac{\partial E_z}{\partial \rho} = -j\omega\mu H_\phi \quad (7)$$

$$E_\rho = \frac{k_z}{\omega\epsilon} H_\phi \quad (8)$$

$$E_z = \frac{1}{j\omega\epsilon} \frac{1}{\rho} \frac{\partial(\rho H_\phi)}{\partial \rho} \quad (9)$$

Substituting (8,9) in (7), one obtains the following differential equation:

$$\frac{d}{d\rho} \left[ \frac{1}{\rho} \frac{d(\rho H_\phi)}{d\rho} \right] + \gamma^2 H_\phi = 0 \quad (10)$$

where  $\gamma^2 = k^2 - k_z^2 = \omega^2 \mu \epsilon - k_z^2$ . Substituting  $x = \gamma\rho$  in this equation results in the Bessel equation

$$\frac{d^2 H_\phi}{dx^2} + \frac{1}{x} \frac{dH_\phi}{dx} + \left(1 - \frac{1}{x^2}\right) H_\phi = 0 \quad (11)$$

with the possible solutions in the form of Bessel, Hankel and modified Bessel functions. The general solutions for the fields  $H_\phi$  and  $E_z$  in layers 1-4 are written in Table 1.

Table 1: General field solutions  $E_z$  and  $H_\phi$  of the waveguide.

Fields (eigenfunctions)	Eigenvalue and constant of propagation
1 $\begin{cases} H_{\phi 1} = C_1 J_1(\gamma_1 \rho) \\ E_{z1} = \frac{C_1 \gamma_1}{j\omega\epsilon_1} J_0(\gamma_1 \rho) \end{cases}$	$\gamma_1^2 = k_1^2 - k_z^2$ $k_1 = \omega\sqrt{\mu_0\epsilon_1}$ $= \omega\sqrt{\mu_0\epsilon_0\epsilon_{r1}}$
2 $\begin{cases} H_{\phi 2} = C_2 J_1(\gamma_2 \rho) + C_3 Y_1(\gamma_2 \rho) \\ E_{z2} = \frac{\gamma_2}{j\omega\epsilon_2} [C_2 J_0(\gamma_2 \rho) + C_3 Y_0(\gamma_2 \rho)] \end{cases}$	$\gamma_2^2 = k_2^2 - k_z^2$ $k_2 = \omega\sqrt{\mu_0\epsilon_2}$ $= \omega\sqrt{\mu_0 \left( \epsilon_0 \epsilon_{r2} + \frac{\sigma_2}{j\omega} \right)}$
3 $\begin{cases} H_{\phi 3} = C_4 J_1(\gamma_3 \rho) + C_5 Y_1(\gamma_3 \rho) \\ E_{z3} = \frac{\gamma_3}{j\omega\epsilon_3} [C_4 J_0(\gamma_3 \rho) + C_5 Y_0(\gamma_3 \rho)] \end{cases}$	$\gamma_3^2 = k_3^2 - k_z^2$ $k_3 = \omega\sqrt{\mu_{r3}\mu_0\epsilon_3}$ $= \omega\sqrt{\mu_{r3}\mu_0 \left( \epsilon_0 \epsilon_{r3} + \frac{\sigma_3}{j\omega} \right)}$
4 $\begin{cases} H_{\phi 4} = C_6 H_1^{(2)}(\gamma_4 \rho) \\ E_{z4} = \frac{C_6 \gamma_4}{j\omega\epsilon_4} H_0^{(2)}(\gamma_4 \rho) \end{cases}$	$\gamma_4^2 = k_4^2 - k_z^2$ $k_4 = \omega\sqrt{\mu_0\epsilon_0} = \omega\sqrt{\mu_0\epsilon_1}$

In Table 1, the parameters  $\mu_0$  and  $\epsilon_0$  are respectively the magnetic permeability and the electric permittivity of the free space,  $\epsilon_1$ - $\epsilon_3$  the electric permittivity of the layers 1-3, and  $\sigma_2$  and  $\sigma_3$  the electric conductivity of the layers 2 and 3,  $\mu_{r3}$  the relative magnetic permeability of the layer 3, and  $\sigma_2$  and  $\sigma_3$  the electric conductivity of the layers 2 and 3. The constants  $C_2$ - $C_6$  can be expressed in terms of  $C_1$ .

## 2.2 Eigenvalue equation

The eigenvalue equation to determine the parameters  $\gamma_1$ - $\gamma_4$  presented in Table 1 is derived in this section. Note that the parameters  $\gamma_1$ - $\gamma_4$  are related to each other, for example  $\gamma_2^2 = \gamma_1^2 + k_2^2 - k_1^2$ . Thus only one of them needs to be calculated, and the others can be easily determined. The parameter chosen in this analysis is  $\gamma_1$ . The procedure to obtain the eigenvalues equation is as follows.

Using the general solutions presented in Table 1 and applying the boundary conditions of continuity of the fields  $E_z$  and  $H_\phi$  at the surfaces  $\rho=a$ ,  $\rho=b$  and  $\rho=c$ , the following set of equations is obtained

$$C_1 J_1(\gamma_1 a) = C_2 J_1(\gamma_2 a) + C_3 Y_1(\gamma_2 a) \quad (12)$$

$$C_2 J_1(\gamma_2 b) + C_3 Y_1(\gamma_2 b) = C_4 J_1(\gamma_3 b) + C_5 Y_1(\gamma_3 b) \quad (13)$$

$$C_4 J_1(\gamma_3 c) + C_5 Y_1(\gamma_3 c) = C_6 H_1^{(2)}(\gamma_4 c) \quad (14)$$

$$\frac{C_1 \gamma_1}{j \omega \varepsilon_1} J_0(\gamma_1 a) = \frac{\gamma_2}{j \omega \varepsilon_2} [C_2 J_0(\gamma_2 a) + C_3 Y_0(\gamma_2 a)] \quad (15)$$

$$\frac{\gamma_2}{j \omega \varepsilon_2} [C_2 J_0(\gamma_2 b) + C_3 Y_0(\gamma_2 b)] = \frac{\gamma_3}{j \omega \varepsilon_3} [C_4 J_0(\gamma_3 b) + C_5 Y_0(\gamma_3 b)] \quad (16)$$

$$\frac{\gamma_3}{j \omega \varepsilon_3} [C_4 J_0(\gamma_3 c) + C_5 Y_0(\gamma_3 c)] = \frac{C_6 \gamma_4}{j \omega \varepsilon_4} H_0^{(2)}(\gamma_4 c) \quad (17)$$

To simplify the notations, the following variables are defined

$$\begin{aligned} x_1 &= J_1(\gamma_1 a), \quad x_2 = J_1(\gamma_2 a), \quad x_3 = Y_1(\gamma_2 a), \quad x_4 = J_1(\gamma_2 b) \\ x_5 &= Y_1(\gamma_2 b), \quad x_6 = J_1(\gamma_3 b), \quad x_7 = Y_1(\gamma_3 b), \quad x_8 = J_1(\gamma_3 c) \\ x_9 &= Y_1(\gamma_3 c), \quad x_{10} = H_1^{(2)}(\gamma_4 c), \quad x_{11} = \frac{\gamma_1}{j \omega \varepsilon_1} J_0(\gamma_1 a) \\ x_{12} &= \frac{\gamma_2}{j \omega \varepsilon_2} J_0(\gamma_2 a), \quad x_{13} = \frac{\gamma_2}{j \omega \varepsilon_2} Y_0(\gamma_2 a), \quad x_{14} = \frac{\gamma_2}{j \omega \varepsilon_2} J_0(\gamma_2 b) \\ x_{15} &= \frac{\gamma_2}{j \omega \varepsilon_2} Y_0(\gamma_2 b), \quad x_{16} = \frac{\gamma_3}{j \omega \varepsilon_3} J_0(\gamma_3 b), \quad x_{17} = \frac{\gamma_3}{j \omega \varepsilon_3} Y_0(\gamma_3 b) \\ x_{18} &= \frac{\gamma_3}{j \omega \varepsilon_3} J_0(\gamma_3 c), \quad x_{19} = \frac{\gamma_3}{j \omega \varepsilon_3} Y_0(\gamma_3 c), \quad x_{20} = \frac{\gamma_4}{j \omega \varepsilon_4} H_0^{(2)}(\gamma_4 c) \end{aligned} \quad (18)$$

Replacing (18) in (12)-(17), the system of linear equations is obtained:

$$\begin{bmatrix} x_1 & -x_2 & -x_3 & 0 & 0 & 0 \\ 0 & x_4 & x_5 & -x_6 & -x_7 & 0 \\ 0 & 0 & 0 & x_8 & x_9 & -x_{10} \\ x_{11} & -x_{12} & -x_{13} & 0 & 0 & 0 \\ 0 & x_{14} & x_{15} & -x_{16} & -x_{17} & 0 \\ 0 & 0 & 0 & x_{18} & x_{19} & -x_{20} \end{bmatrix} \begin{bmatrix} C_1 \\ C_2 \\ C_3 \\ C_4 \\ C_5 \\ C_6 \end{bmatrix} = \begin{bmatrix} 0 \\ 0 \\ 0 \\ 0 \\ 0 \\ 0 \end{bmatrix} \quad (19)$$

It can be written compactly as  $[x] \times [C] = [0]$ . The constants  $C_2$ - $C_6$  are expressed in terms of  $C_1$ :

$$C_2 = C_1 \frac{(x_1 x_{13} - x_3 x_{11})}{x_2 x_{13} - x_{12} x_3} \quad (20)$$

$$C_3 = C_1 \frac{(x_2 x_{11} - x_1 x_{12})}{x_2 x_{13} - x_{12} x_3} \quad (21)$$

$$C_4 = \frac{d_1 x_{17} - d_2 x_{17}}{x_6 x_{17} - x_{16} x_7} \quad (22)$$

where  $d_1 = C_2 x_4 - C_3 x_5$  and  $d_2 = C_2 x_{14} - C_3 x_{15}$

$$C_5 = \frac{d_2 x_6 - d_1 x_{16}}{x_6 x_{17} - x_{16} x_7} \quad (23)$$

$$C_6 = \frac{C_4 x_8 - C_5 x_9}{x_{10}} \quad (24)$$

The system (19) possesses a nontrivial solution if and only if the determinant of  $[x]$  is null, i.e.

$$\det[x] = 0 \quad (25)$$

This is the eigenvalue equation and its solution gives the eigenvalue  $\gamma_1$ . The parameters  $\gamma_2$ - $\gamma_4$  expressed as functions of  $\gamma_1$  are

$$\gamma_2^2 = \gamma_1^2 + \omega^2 \mu_0 (\varepsilon_2 - \varepsilon_1) \quad (26)$$

$$\gamma_3^2 = \gamma_1^2 + \omega^2 \mu_0 (\mu_{r3} \varepsilon_3 - \varepsilon_1) \quad (27)$$

$$\gamma_4^2 = \gamma_1^2 + \omega^2 \mu_0 (\varepsilon_4 - \varepsilon_1) \quad (28)$$

In order to solve (25), the following normalizations of (26)-(28) are used:

$$\gamma_1 a = \xi \quad (29)$$

$$\gamma_2 a = \sqrt{\xi^2 + (k_0 a)^2 (\varepsilon_{R2} - \varepsilon_{r1})} \quad (30)$$

$$\gamma_2 b = \left(\frac{b}{a}\right) \sqrt{\xi^2 + (k_0 a)^2 (\varepsilon_{R2} - \varepsilon_{r1})} \quad (31)$$

$$\gamma_3 b = \left(\frac{b}{a}\right) \sqrt{\xi^2 + (k_0 a)^2 (\mu_{r3} \varepsilon_{R3} - \varepsilon_{r1})} \quad (32)$$

$$\gamma_3 c = \left(\frac{c}{a}\right) \sqrt{\xi^2 + (k_0 a)^2 (\mu_{r3} \varepsilon_{R3} - \varepsilon_{r1})} \quad (33)$$

$$\gamma_4 c = \left(\frac{c}{a}\right) \sqrt{\xi^2 + (k_0 a)^2 (\varepsilon_{R4} - \varepsilon_{r1})} \quad (34)$$

where  $k_0 = \omega \sqrt{\mu_0 \varepsilon_0} = k_4$ ,  $\varepsilon_{R2} = \varepsilon_{r2} + \sigma_2 / j \omega \varepsilon$ ,  $\varepsilon_{R3} = \varepsilon_{r3} + \sigma_3 / j \omega \varepsilon$ , and  $\varepsilon_{R4} = 1$ . Substituting (29)-(34) in (25), the resulting equation becomes a function of  $\xi$ . As the elements of the matrix  $[x]$  are complex, the solutions  $\xi$  are also complex numbers, with the real part  $\xi_r$  and the imaginary part  $\xi_i$ . With these notations, (25) is a system of two equations and two unknowns:  $\xi_r$  and  $\xi_i$ :

$$\begin{cases} F_1(\xi_r, \xi_i) = \text{Re}(\det[x]) = 0 \\ F_2(\xi_r, \xi_i) = \text{Im}(\det[x]) = 0 \end{cases} \quad (35)$$

The solutions of (35) are the points where the curves  $F_1$  and  $F_2$  are crossed.

### 3. Numerical results and discussions

To solve the system (35), a computer code in the software Matlab was developed. Using this program, the eigenvalues  $\gamma_1$  of the modes  $TM^z$ , the electromagnetic fields, and the current densities can be calculated. The input data in this code are the electromagnetic and geometric parameters of the waveguide and the frequency.

In order to verify the developed code, some results of calculations for two waveguides with the known solutions are presented: the circular metallic waveguide and the circular dielectric waveguide. They are particular cases of the four-layer structure.

#### 3.1 Circular metallic waveguide

The simulation of this waveguide by the developed software can be done choosing the values of the radius  $b$  and  $c$  close to the radius  $a$ , and setting a perfect dielectric in the region 1 (Fig. 1b). One simulation was performed for this waveguide. The parameters of the waveguides used in the simulation are given in Table 2.

Fig. 2 shows the  $F_1$  and  $F_2$  curves obtained for the simulation (Table 2), and Fig. 3 shows the variation of  $K_z/K_0$  versus  $2a/\lambda_0$  ( $\lambda_0$  is the wavelength in free space) for two modes.

Table 2: Input data for the simulation of the metallic waveguide.

Region	$\epsilon_r$	$\sigma$ (S/m)	Radius	Relative permittivity
1	10	0	$a=0.5\text{mm}$	1
2	2	$3.8 \times 10^7$	$b=0.55\text{mm}$	1
3	3	$3.8 \times 10^7$	$c=0.6\text{mm}$	1
4	1	0	-	1

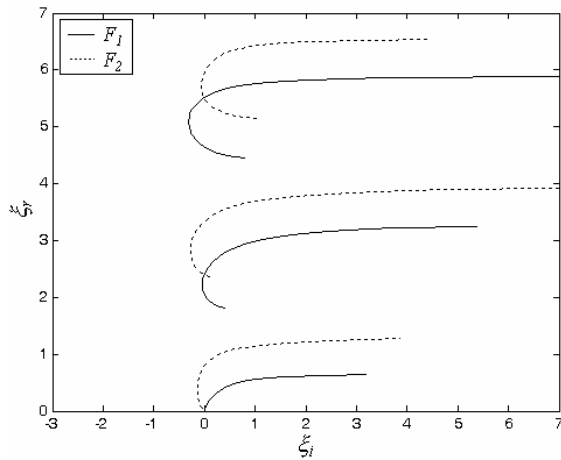


Figure 2. Curves  $F_1$  and  $F_2$  obtained from simulation for the waveguide in Table 2.

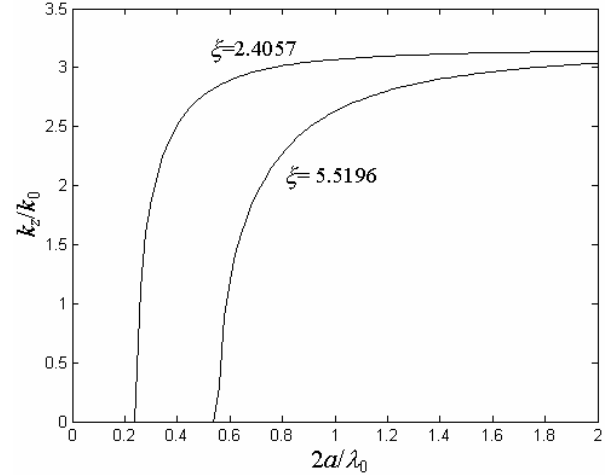


Figure 3. Dispersion curves obtained from the simulation for the waveguide in Table 2.

Fig. 2 shows that in the range  $0 < \xi < 7$ , the eigenvalue solutions for the waveguide are  $\xi = 0, 2.4057$  and  $5.5196$ . The second and the third eigenvalues are in agreement with the ideal circular metallic waveguide, but the value  $\xi = 0$  does not exist in the case of the ideal metallic waveguide. This eigenvalue appears due to the finite conductivity ( $\sigma = 3.8 \times 10^8$  S/m) of the metal, which produces finite electric field inside the conductors for low and medium frequencies. This means that there is no cutoff frequency for this mode  $TM^z$ . In other words, at low frequencies only this mode propagates. In this work, this mode is denoted by  $TM^z_{00}$ .

#### 3.2 Circular dielectric waveguide

The simulation for this waveguide was done setting the values of the radius  $b$  and  $c$  close to the radius  $a$ , and setting a perfect dielectric on the layers 1-4, but with different relative permittivity (Fig. 1). The parameters used for calculations are given in Table 3. The obtained results are shown in Figs. 4 and 5. Again, the results agree with the known ones.

Table 3: Input data for the simulation of the dielectric waveguide.

Region	$\epsilon_r$	$\sigma$ (S/m)	Radius	Relative permittivity
1	20	0	$a=0.5\text{mm}$	1
2	2	0	$b=0.505\text{mm}$	1
3	3	0	$c=0.51\text{mm}$	1
4	1	0	-	1

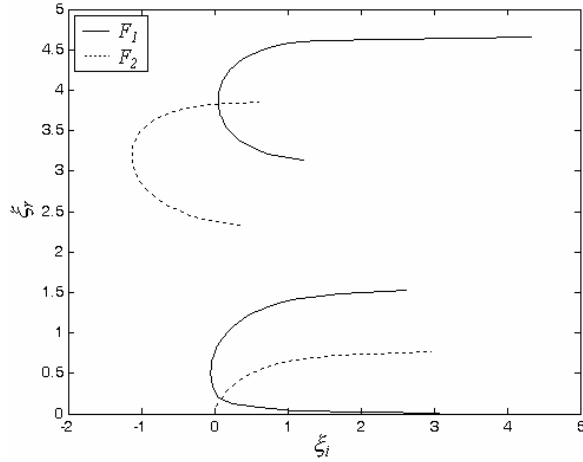


Figure 4. Curves  $F_1$  and  $F_2$  obtained from simulation for the waveguide in Table 3.

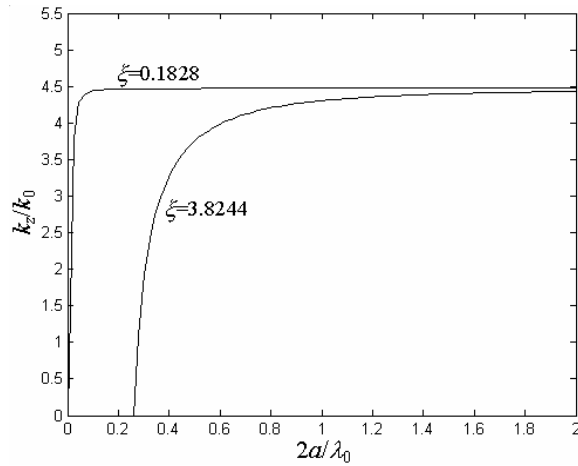


Figure 5. Dispersion curves obtained from simulation 1 of the waveguide in Table 3.

### 3.3 OPGW waveguide

The simulation of this waveguide was done using a perfect dielectric in the region 1 (Fig. 1), and the regions 2 and 3 as nonideal conductors. The materials used in the waveguide are shown in Fig. 1. The electromagnetic and geometric parameters are given in the Table 4.

Table 4: Input data for the simulation of the OPGW waveguide.

Region	$\epsilon_r$	$\sigma$ (S/m)	Radius	Relative permittivity
1	3.8	0	$a=2.35\text{mm}$	1
2	1	$3.96 \times 10^7$	$b=4.35\text{mm}$	1
3	1	$0.2 \times 10^7$	$c=7.00\text{mm}$	1000
4	1	0	-	1

### 3.3.1 Eigenvalues and dispersion curves

Fig. 6 shows the calculated curves  $F_1$  and  $F_2$  for  $f = 1.2$  kHz. The crossing points give the eigenvalues  $\xi = 0$  and  $2.4048$  for this frequency. Again, the mode  $\text{TM}^z_{00}$  is present in this waveguide. Fig. 7 shows the dispersion curves obtained for the waveguide. Using this figure, it is possible to calculate the cutoff frequency corresponding to the eigenvalue  $\xi = 2.4048$ . The value of this frequency is 25.5 GHz, and the cutoff frequencies of the other superior modes are greater. For this reason, the only mode that propagates at low frequencies is the  $\text{TM}^z_{00}$ . The next sections present the analysis of this mode.

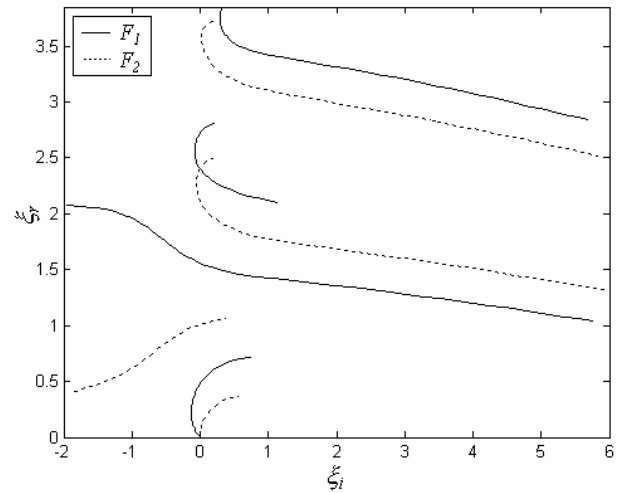


Figure 6. Curves  $F_1$  and  $F_2$  obtained from simulation for the OPGW waveguide in Table 4 for  $f = 1.2\text{kHz}$ .

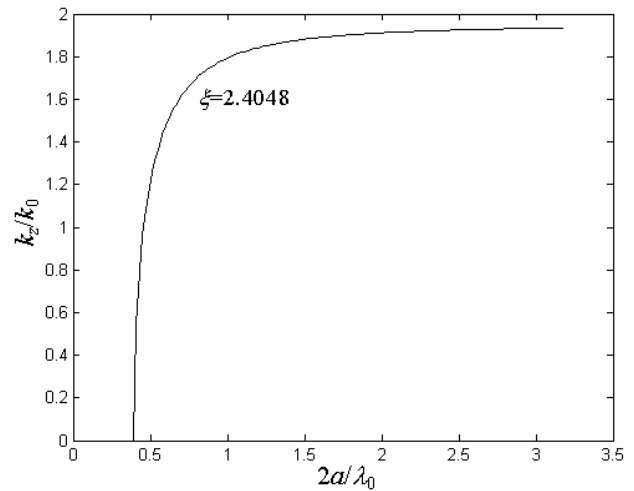


Figure 7. Dispersion curves obtained from the simulation of the OPGW waveguide in Table 4.

### 3.3.2 Electromagnetic field distribution

Fig. 8 shows the variation of the electric field  $E_z$  versus the radial coordinate  $\rho$  for the frequencies 0.1, 0.25, 0.5, and 1.0 kHz. These curves show that when the frequency increases the electric field inside the waveguide diminishes.

The distribution of the magnetic field  $H_\phi$  as a function of  $\rho$  for different frequencies is presented in Figs. 10 and 11. This field inside the waveguide is also reduced with increasing frequency.

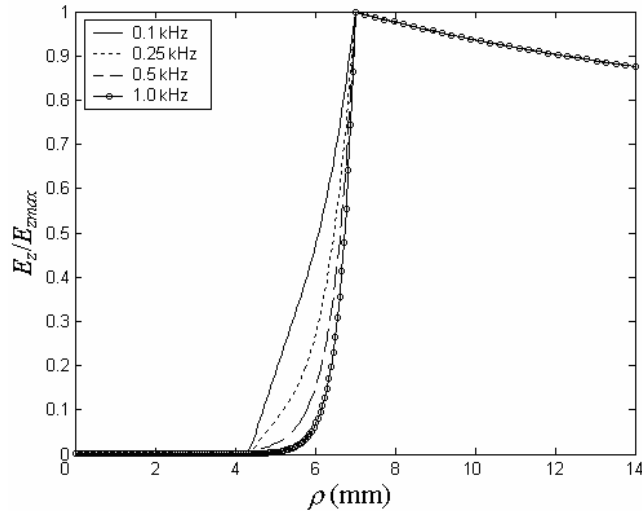


Figure 8. Magnitude of the electric field  $E_z$  versus the radial coordinate.

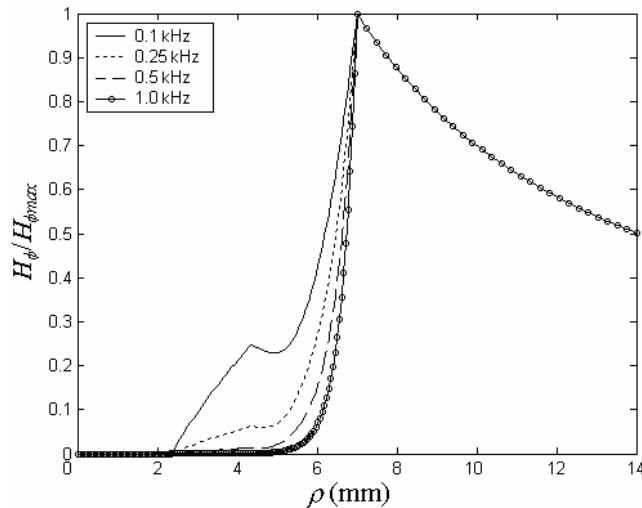


Figure 9. Magnitude of the magnetic field  $H_\phi$  versus the radial coordinate.

### 3.3.3 Current density distributions

The variation of the magnitude of the current density  $J_z$  as a function of the radial coordinate  $\rho$  of the waveguide is shown in Figs. 10 and 11. These figures present the results calculated both by the Matlab code and the commercial Finite Element Method Femlab software. The phase variation of this current density is presented in Fig. 12.

These results show that at the frequency of 100 Hz and below this value, the current distribution in the layer 2 ( $2.35 \text{ mm} < \rho < 4.35 \text{ mm}$ ) is considerable and approximately constant along this layer. For frequencies larger than 1 kHz (Fig. 11) the skin effect in the layer 3 ( $4.35 \text{ mm} < \rho < 7.0 \text{ mm}$ ) appears, so that at the frequency  $f = 70 \text{ kHz}$  the current density practically exists only at the surface of the external conductor (surface of the steel layer).

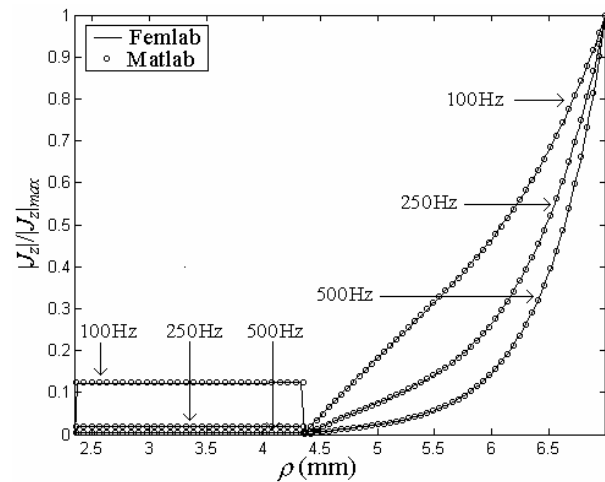


Figure 10. Magnitude of the current density  $J_z$  versus the radial coordinate.

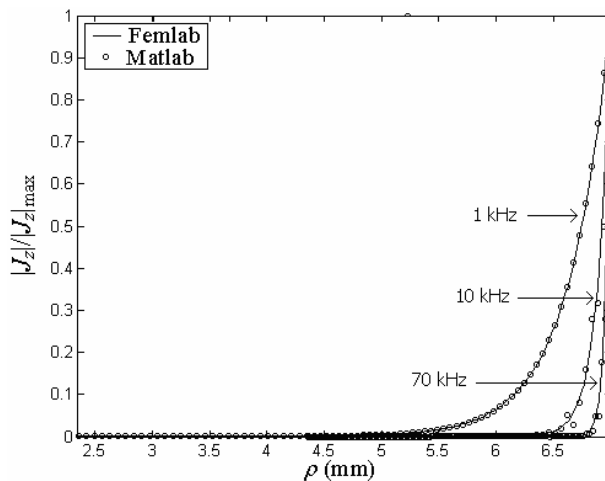
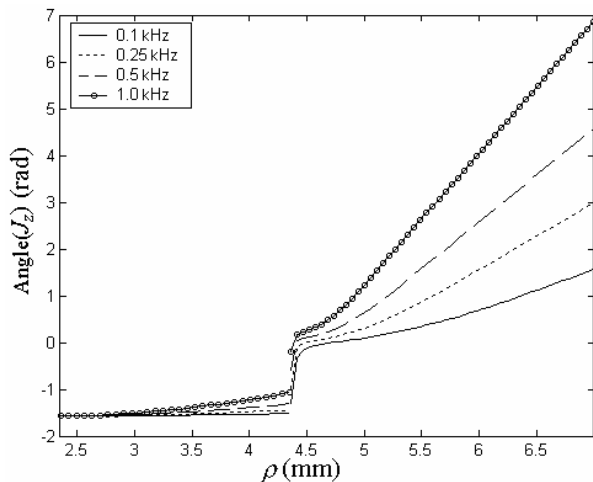


Figure 11. Magnitude of the current density  $J_z$  versus the radial coordinate.





**Figure 12. Phase of the current density  $J_z$  versus the radial coordinate.**

It is observed that the results of skin effect in Fig. 11 are in agreement with the approximated equation of the skin depth ( $\delta = (\pi f \mu \sigma)^{-1/2}$ ). For example, at  $f = 1$  kHz,  $\delta = 0.36$  mm, and this skin depth corresponds to  $\rho = 6.6$  mm and  $|J_z(6.6\text{mm})|/|J_{z|\text{max}}| = 0.37 \approx e^{-1}$  (Fig. 11).

#### 4. Conclusions

This paper presents an analytical model based on the exact solution of Maxwell's equations in the frequency domain for analysis of multi-conductor cables. The OPGW cable was considered as a circular waveguide with four layers: dielectric, aluminum, steel and air.

The main results of this work are as follows. An analytical waveguide model and a correspondent computational program were developed, which allow for the calculation of the electromagnetic field and current distributions in cables consisting of azimuthally uniform layers with nonideal materials, i.e. with metals with finite conductivity and dielectrics with losses. This model allows one, in particular to investigate the skin effect and the electromagnetic fields inside and outside the cables.

The algorithm is verified by comparing it with two known exact solutions of waveguide problems and with the solutions for current density distribution obtained by the Finite Element Method using the commercial program Femlab.

To the knowledge of the authors it is the first time that this method is applied to the OPGW cable problem, and it can be extended to other possible cable configurations which could improve current density and temperature distributions to minimize the unwanted effects mentioned in the introduction.

#### 5. References

[1] S. Colle, M. A. Andrade, J. T. Pinho, J. C. V. da Silva, M. Bedia, C. E. Veigal, and J. N. Scussel, "Temperature Response of OPGW with Armored Aluminum Covered Steel Wires Submitted to Short-Circuit", accepted for publication in 2006 IWCS/Focus Conference.

[2] Z. Miro, J. Franc and T. Igor, "Skin effect impact on current density distribution in OPGW cables", *Electrotechnical Review*, Vol. 70, pp. 17 - 21, 2003.

[3] J. Franc, Z. Miro, T. Igor and U. Ivo, "Distribution of current density in layers of overhead bare conductors", *Power System and Communications Infrastructures for the Future*, Beijing, September 2002.



Karlo Queiroz da Costa was born in Belém, Pará, Brazil, on September 5, 1977. He received the B.Sc., M.Sc, and Dr. degree in electrical engineering from the Universidade Federal do Pará (Brazil) respectively in 2001, 2002, and 2006. He has joined with the Department of Electrical Engineering of the Federal University of Pará in 2006 as professor of applied electromagnetism.

His research interests are centered on applied electromagnetics, microwaves, antennas, propagation, numerical methods, and grounding systems. In these areas he has published many papers in conferences and periodicals.



Victor Dmitriev was born in Russia, in 1947. Currently, he is a professor at the Federal University of Para, Belem, Brazil. Dr. Victor Dmitriev has more than 120 papers in scientific journals, several books and patents. The fields of his scientific interest are microwave, millimeter wave and optic components, application of group theory to electromagnetic problems, complex media, nanophotonics, and mathematical methods of electromagnetic theory.



João Tavares Pinho was born in Belém, Pará, Brazil, on August 22, 1955. He received the B.Sc. degree in electrical engineering from the Universidade Federal do Pará (Brazil) in 1977, the M.Sc. degree in electrical engineering from the Pontificia Universidade Católica do Rio de Janeiro (Brazil) in 1984, and the Dr.-Ing. degree in electrical engineering from the Rheinisch-Westfälische Technische Hochschule Aachen (Germany) in

1990. He has been with the Department of Electrical Engineering of the Universidade Federal do Pará since 1978, has worked as an assistant at the RWTH Aachen, was the coordinator of the post-graduation course in electrical engineering at the UFPA from 1992 to 1994, and is presently a full professor and leader of a research group on energy alternatives and microwave applications. His research interests have been centered on electromagnetics, especially on microwave applications, and on the application of hybrid systems for the generation of electricity, especially those involving photovoltaic and wind energy. In these areas he has supervised many graduate and undergraduate works and published several papers. Prof. Pinho is ad hoc advisor for several committees and institutions in Brazil, member of various scientific societies, former president of the Brazilian Microwave and Optoelectronics Society, and presently president of the Brazilian Section of the International Solar Energy Society.



Prof. Sergio Colle

LEPTEN – Department of Mechanical Engineering – UFSC (Federal University of Santa Catarina)

88040-900 – Florianópolis – SC – Brazil

Bibliography:

Mechanical Engineer degree in 1970 - UFSC

Master of Science in Mechanical Engineering in 1972 – COPPE / University of Rio de Janeiro

Doctor of Science in Mechanical Engineering in 1976 – COPPE / University of Rio de Janeiro

Professor of Thermodynamics, Heat Transfer and Solar Energy – Department of Mechanical Engineering – UFSC since 1974

He is presently head of LEPTEN.



Luciana Pereira Gonzalez was born in Belém, Para, Brazil in 1977. She graduated in Electrical Engineering at the Federal University of Pará (UFPA) in May of 2006. She is now a postgraduate student at UFPA.



Marcelo de Araujo Andrade was born in Florianópolis – SC – Brazil in 1965. He graduated in Mechanical Engineer from Universidade Federal de Santa Catarina in 1988. He joined Prysmian Telecomunicações Cabos e Sistemas do Brasil in 1988 and actually he is in charge of Comercial and R&D Direction.



João Carlos Vieira da Silva was born in São Paulo – SP – Brazil in 1959. He graduated in BSc Physics from Universidade de São Paulo in 1982 and Electrical Engineer from Faculdade de Engenharia de Sorocaba in 1991. He joined Prysmian Telecomunicações Cabos e Sistemas do Brasil in 1977 and actually he is in charge of Product Engineering Department.



Mauro Bedia Jr. was born in São Paulo – SP – Brazil in 1970. He graduated in Mechanical Engineer from Faculdade Santa Cecília in 1996. He joined Prysmian Telecomunicações Cabos e Sistemas do Brasil in 1989 and actually he is responsible for OPGW and ADSS cable development.





## **International Wire & Cable Symposium (IWCS) Inc.**

*174 Main Street,  
Eatontown,  
New Jersey 07724  
USA*

*Telephone - +1-732-389-0990; Fax - +1-732-389-0991*

[www.iwcs.org](http://www.iwcs.org)

*Editor: Dr Alistair Duffy  
De Montfort University, Leicester UK*